Interfacial Stabilization of Metastable TiO_2 Films

Daniel G. Gregory,[†] Li Lu,[‡] Christopher J. Kiely,[†,‡] and Mark A. Snyder[*,†]

[†]Department of Chemical and Biomolecular Engineering and [‡]Department of Materials Science and Engineering, Lehigh University, Bethlehem, Pennsylvania 18015, United States

[*] Supporting Information

ABSTRACT: This work demonstrates a phenomenon that preserves the traditionally metastable anatase crystal structure of thin titania (TiO_2) films along a two-dimensional oxide interface at temperatures well in excess of those that normally trigger a full polymorphic transformation to rutile in higher dimensionality crystalline powders. Whereas atomic surface mobility appears to dominate polymorph transformation processes within bulk TiO_2 powders, a simple reduction in dimen-sionality to a two-dimensional TiO_2 film (ca. 50−200 nm thick), supported upon a substrate, leads to a remarkable resistance to the calcination-induced anatase-to-rutile transformation. This stabilization does not appear to be specifically reliant on substrate character given its persistence for TiO_2 films prepared on amorphous silica (SiO_2) as well as crystalline TiO_2 substrates. Instead, interface-mediated coordination of the TiO_2 film with the substrate, and the inherent confinement of crystallites in two dimensions, is believed to resist polymorph transformation by mitigation of the atomic surface mobility. Only when temperatures (i.e., >800 °C) that are conducive to bulk atomic mobilization are reached does reconstructive grain growth convert the film into the thermodynamically stable rutile crystal structure.

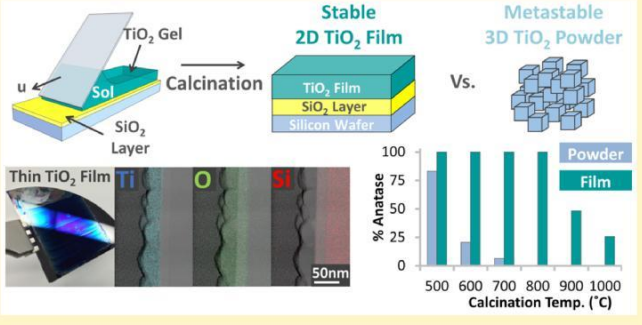

INTRODUCTION

Transition metal oxide films are utilized in a wide range of applications including catalysis, dye-sensitized solar cells (DSSC), pollution abatement technologies, gas sensors, and hydrothermally stable protective layers.[1−3] The unique chemical, electronic, optical, and structural character of transition metal oxides establishes a diverse palette of materials that offer selective control of properties including refractive index,[4] roughness,[5,6] gas permeability,[7] band gap,[8] catalytic perform-ance,[9,10] and stability,[11] among others. The inherent low surface energies characteristic of most oxides enable increased atomic surface mobility, permitting them to spread and coat substrates at moderate temperatures.[12] These properties allow oxides to be readily dispersed as films with tunable thicknesses but also make oxides susceptible to structural reconfiguration at relatively low temperatures.

Oxide films are typically synthesized using a chemical precursor that is deposited onto a substrate via dip coating,[13] convective deposition,[14] spin coating,[15] or atomic layer deposition.[16] Calcination of the resulting precursor film at elevated temperatures ($T > 400$ °C) to promote crystallization also triggers processes of hydrolysis, condensation, syneresis, polymorph transformation, and sintering[17] that can alter the structure and inherent properties of the film. Specifically, hydrolysis, condensation, and densification occurring during syneresis[18−23] typically result in the formation of a porous matrix of interconnected crystallites on the order of ~10−100 nm, as opposed to large single crystal monoliths. At higher temper-atures, additional methods of thermal reconstruction occur, including sintering, atomic surface migration, and polymorphic transformation.[24] These processes can be problematic in film preparation, given the continuous reconfiguration of the topological and chemical structure of the film with heating.

Oxides often undergo a polymorphic transformation from a metastable crystal structure (e.g., anatase in titania) to a more stable crystal structure (e.g., rutile in titania) above ~500 °C.[25] This process typically initiates at the material's surface, as opposed to within the bulk of the crystalline lattice, as the surface of the oxide is not fully coordinated to a rigid crystalline matrix of neighboring atoms, but rather with a diverse range of surface species (e.g., M−OH, $M(O)_x$, M−O−M, where M denotes a metal).[26] As a result, surface atoms are bound with less cohesive energy than bulk lattice atoms and are more readily able to mobilize, reconfigure, and even disorder at low temperatures.[27,28] This reduced level of cohesion invites the development of surface relaxation, defect sites, and surface amorphization during calcination, all of which are likely to assist in the propagation of polymorph transformations from the surface of the oxide. As such, it is sometimes desirable to limit the surface area of the material in order to preserve metastable crystalline states.

The most widely recognized method of preventing polymorph evolution from occurring in bulk oxides entails the use of aliovalent dopants (e.g., Y^{3+}, Ca^{2+}, Mg^{2+}, etc.) to relax

internal strains within a crystal and to prevent polymorph transformations from propagating throughout the bulk of the crystalline lattice.[29] Another widely discussed method of preserving metastable crystal structures is to reduce the crystallite size below a critical radius in order to effectively balance the surface and bulk free energies.[30−32] Similarly, polymorph stabilization has been reported by maintaining coherency along intercrystalline grain boundaries in fully densified materials. This interfacial contact is reported to induce a boundary strain upon neighboring crystallites that prevents polymorph transformations.[33−35]

Direct epitaxial growth of metastable oxide phases in registry with the lattice of a crystalline substrate has been shown to promote stabilization by limiting porosity and surface area of the film and by increasing coherency of neighboring crystallites.[36] While this has been achieved by metal−organic chemical vapor deposition (MOCVD), which requires an elaborate experimental apparatus, adequate environmental control, and the use of pristine single crystal substrates, similar stabilization phenomena have been observed on crystalline Si(100) surfaces prepared via more rapid dip coating and spin coating techniques.[37,38] In these latter systems, however, characterization of the mechanism of stabilization is lacking, and the possibility of a native oxide layer (SiO_2) existing along the surface of the substrate (SiO_2/Si wafer) has yet to be fully characterized.

In this work, we seek to elucidate fundamental mechanistic insight into the stabilization of supported oxide films. This is accomplished by examining the crystalline polymorphism of thin TiO_2 films in the ~50−200 nm thickness range, deposited directly on the amorphous surface layer of thermally oxidized silicon wafers (TiO_2/SiO_2/Si wafer) via a facile convective deposition process. We draw direct comparisons with the polymorphism of bulk crystalline powders prepared from the same chelated TiO_2 precursor and quantify the resistance to the anatase-to-rutile transformation accompanying the reduction in dimensionality to two-dimensional thin films. In each case, we frame the analysis of the TiO_2 polymorphism by comparisons with the characteristic Hüttig and Tammann temperatures, defining respectively the onset of surface and bulk-to-surface atomic mobility for bulk systems.[24] Correlation of polymorphism to crystallite size, film thickness, and substrate composition provides mechanistic insight into the critical role that interfacial coordination and two-dimensional crystallite confinement play in stabilizing metastable oxide films.

EXPERIMENTAL METHODS

Materials. The following reagents were obtained from Sigma-Aldrich and used without further purification: sulfuric acid (H_2SO_4, 98 wt %), ethyl acetoacetate (CH_3COCH_2CO-OC_2H_5, ≥99.8 wt %), 2,4-pentadione ($CH_3COCH_2COCH_3$, >99 wt %), 2,3-butanedione ($CH_3COCOCH_3$, 97 wt %), and titanium(IV) butoxide ($Ti(OBu)_4$, 97 wt %). Hydrogen peroxide (H_2O_2, 30 wt %) and 200 proof ethanol were obtained from Fisher Scientific. Single crystal silicon (100) wafers were purchased from Silicon Quest International.

Substrate Preparation. The commercial silicon (Si) wafers were used as a supporting substrate for the deposition of titania films. Prior to film deposition, the wafers were immersed in a piranha solution (98 wt % sulfuric acid mixed with 30 wt % hydrogen peroxide in a 3:1 volume ratio) for at least 12 h in order to remove organic surface residue and to simultaneously hydroxylate the surface. The cleaned wafers were rinsed with deionized water followed by the growth of a thermal oxide layer through calcination at 800 °C (ramp rate of 5 °C/min) in air for a soak time of 3 h.

Preparation of Film and Powder Precursor Solutions. Stabilized TiO_2 precursor solutions[39] were prepared by first mixing ethyl acetoacetate (EAA), 2,4-pentadione (PD), and 2,3-butanedione (BD) in a sealed container, followed by addition of titanium(IV) butoxide ($Ti(OBu)_4$) under vigorous stirring and dilution with ethanol (EtOH) to reach a final molar composition of 8 EAA/1 PD/1 BD/14 $Ti(OBu)_4$/641 EtOH. The stabilized precursor solution was then vigorously stirred for at least 1 h prior to bulk TiO_2 production or film deposition.

Bulk TiO_2 Production and Convective Deposition of Titanium Oxide Films. Bulk TiO_2 powders were prepared by evaporating excess solvent from a 3 mL aliquot of the chelated TiO_2 precursor solution in a fume hood over the course of 24 h. The residual gel was then calcined (ramp rate of 5 °C/min) at a systematic series of temperatures ranging from 500 to 1000 °C, utilizing a 3 h soak time. Thin TiO_2 films with tunable thickness were deposited via convective deposition onto the oxidized silicon wafers using a modified syringe pump apparatus as reported elsewhere.[40] Generally, oxidized wafers were mounted horizontally, and the linear motor of the syringe pump was used to drive the substrate at a rate, u [cm min^{-1}], relative to a glass slide mounted at a 45° angle above the substrate. The edge of the glass slide parallel to the substrate was covered with a piece of Parafilm. A 20−50 μL aliquot of the chelated TiO_2 precursor solution was dispensed in the angle between the coating blade and substrate, where it was held as a meniscus pinned to the blade and substrate during the coating process. Drawing of the substrate at rates of 0.12−1.2 cm min^{-1} led to deposition of the precursor solution along the oxidized silicon wafer, where solvent evaporation at the contact line of the meniscus with the substrate led to gelation of the alkoxide-based TiO_2 precursor film. Calcination of the deposited film was carried out at a systematic series of temperatures ranging from 500 to 1000 °C (ramp rate of 5 °C/min) with a 3 h soak time.

Powder and Film Characterization. Ellipsometry measurements were conducted on the Si wafers to measure the thickness of the thermally grown oxide layer using a V-vase variable angle spectroscopic ellipsometer (J.A. Woollam Company, Inc.). The data obtained were analyzed using the WVASE32 software package (Figure S1). After preparing the TiO_2 films on the SiO_2/Si substrate, TiO_2 crystallinity was examined using a Rigaku Miniflex II X-ray diffractometer with Cu Kα radiation ($\lambda_{K\alpha}$ = 1.5418 Å). Calculation of the volume percentage of the anatase fraction of the crystal structure was performed by integrating the characteristic peak intensities of each corresponding polymorph (i.e., the rutile (110) peak, I_R, at 2θ ~ 27.5° and anatase (101) peak, I_A, at 2θ ~ 25.3°) according to $100 \times [0.79I_A/(I_R + 0.79I_A)]$, where I_i is the integrated intensity of the reflection corresponding to polymorph i.[41] XRD Scherrer analysis was carried out to qualitatively assess the mean crystallite size, τ, based upon the characteristic peak intensity of each polymorph, by $\tau = K\lambda/(\beta \cos \theta)$, where K is the shape factor, λ is the wavelength, β is the line broadening at full width at half-maximum intensity, and θ is the Bragg angle.[42]

Prior to imaging via scanning electron microscopy (SEM), samples mounted onto an Al stub were first coated with ~4 nm of iridium using a plasma deposition instrument to avoid charging. SEM images were collected using a Hitachi 4300 SE/N SEM instrument operating at accelerating voltages ranging

from 5 to 10 kV. Transmission electron microscopy (TEM) was performed with a JEOL 2000FX microscope at 200 kV. Scanning transmission electron microscopy (STEM) was carried out at an accelerating voltage of 200 kV using an aberration corrected JEOL JEM-ARM-200CF microscope equipped with a Centurio X-ray energy dispersive X-ray (XEDS) system. Focused ion beam (FIB) milling (Figures S2 and S3) was performed using an FEI Scios DualBeam FIB to prepare electron transparent cross-section slices of the calcined $TiO_2/SiO_2/Si$ wafers.

RESULTS AND DISCUSSION

Mechanistic Insight into Polymorphic Transformation of Bulk Crystalline TiO_2 Powders. As shown through X-ray diffraction in Figure 1a, bulk titania powders, prepared through

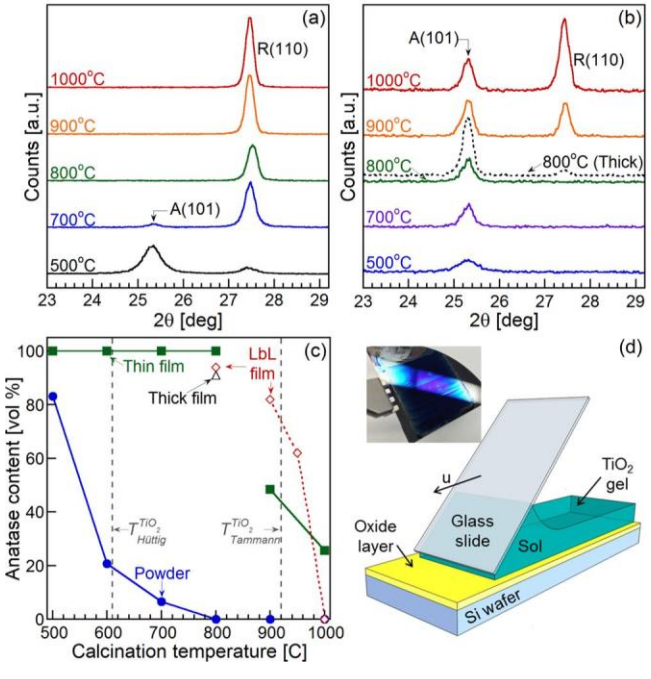

Figure 1. X-ray diffraction (XRD) of TiO_2 (a) powders and (b) films after 3 h calcination at specified temperatures. Powders in (a) were prepared by bulk solvent evaporation from a chelated TiO_2 precursor. Films in (b) were prepared by (d) blade coating aliquots of the chelated TiO_2 precursor solution onto a thermally grown oxide layer of a silicon wafer at rates of $u = 1.2$ cm min^{-1} (50 μL) to yield "thin" films (solid lines) and $u = 0.12$ cm min^{-1} (50 μL) to yield "thick" films (dashed line). The temperature-dependent volume percentage of anatase TiO_2 within the powder (closed circles) and films (thin: closed squares; thick: open triangles), estimated from integrated rutile, R(110), and anatase, A(101), reflections, is compared in (c) with characteristic Hüttig and Tammann temperatures for bulk TiO_2 shown for reference. Anatase volume fractions are also shown in (c) for thicker films derived from layer-by-layer (LbL) coatings (open diamonds) prepared by 10 sequential blade coatings of 20 μL of the chelated TiO_2 solution ($u = 1.2$ cm min^{-1}) with intermediate 3 h calcination at 800 °C and final calcination at the specified temperatures.

calcination of chelated TiO_2 gels to temperatures spanning 500−1000 °C, undergo a characteristic transformation from the metastable anatase (A) polymorph to the thermodynamically stable rutile (R) polymorph. This well-characterized transformation between the two most common TiO_2 polymorphs is indicated by the gradual disappearance of the characteristic A(101) reflection in favor of the R(110) reflection and corresponds to an increase in the volume fraction of rutile TiO_2 at the expense of the anatase TiO_2 component (Figure 1c).

The evolution of the anatase volume fraction as a function of calcination temperature reveals that most of the polymorphic change occurs by ca. 600 °C in the powder sample. The similarity of this transition temperature with the characteristic Hüttig temperature of bulk crystalline titania (TiO_2 $T_{Hüttig}$ ~ 610 °C), namely the temperature marking the onset of atomic surface mobility, underscores the reconstructive nature of the anatase-to-rutile transformation. These TiO_2 powders consist of aggregates of small primary crystallites about 20−40 nm in size. This high surface area morphology is conducive for enhanced surface-localized atom mobility, which aids the reconstructive transformation to rutile.

Mechanistic Insight into the Polymorphic Transformation Behavior of TiO_2 Thin Films. Convective deposition, or blade coating (schematized in Figure 1d), of the chelated $Ti(OBu)_4$ precursor solution onto an oxidized silicon wafer offers a facile route toward the preparation of uniform thin (ca. 50−200 nm) TiO_2 films. This simple reduction in dimensionality of the TiO_2 gel from a three-dimensional bulk powder, into a two-dimensional film, wields a remarkable influence on the calcination-induced polymorphism. Specifically, XRD of thin TiO_2 films (Figure 1b), prepared by blade-coating at a rate, u, of 1.2 cm/min and subsequent calcination at various temperatures between 500 and 1000 °C, reveals a marked impedance of the anatase-to-rutile polymorphic transition, which was characteristic in the TiO_2 bulk samples (Figures 1a,c).

Figures 1b,c show that in film form TiO_2 ultimately starts as 100% anatase under mild calcination temperatures of 500 °C. The integrity of the anatase polymorph persists in the thin films calcined up to 800 °C, the temperature by which the bulk powder (Figures 1a,c) had undergone a complete conversion to the rutile form of TiO_2. In fact, in the case of the thin films, only when the calcination temperature is raised to 900 °C, a temperature commensurate with the onset of bulk-to-surface atomic mobility and defined as the Tammann temperature for bulk TiO_2 (Figure 1c), does the anatase-to-rutile polymorphic transition begin to occur. This transformation is indicated by the appearance of the R(110) reflection and results in an ~50% reduction in anatase content. However, despite a progressive increase of the rutile volume fraction with calcination temperature, the TiO_2 films never fully transform to pure rutile at the highest temperature studied here (i.e., 18% anatase remained after calcination at 1000 °C). Thus, this delayed onset of the expected polymorph transformation suggests that oxide confinement into a two-dimensional film mitigates the influence of atomic surface mobility on the polymorphic transformation. This stabilization phenomenon finally begins to break down when the calcination temperature is increased to the point where bulk-to-surface atom mobility becomes significant.

The cross-sectional TEM image, corresponding XEDS line scans (Figure 2), and area maps (Figure S4) show that the stabilized titania film sits atop a thermally grown amorphous oxide layer covering the silicon wafer. The TiO_2 film in this sample, which was calcined to 800 °C, is approximately 40 nm thick and is supported on a 25 nm thick SiO_2 (thermal oxide) layer. While the oxide layer was purposefully pregrown prior to TiO_2 film deposition, ellipsometry shows that the SiO_2 layer also increases in thickness beneath the TiO_2 film during the high-temperature calcination treatment (Figure S1). Whereas similar polymorphic stabilization phenomena have been observed

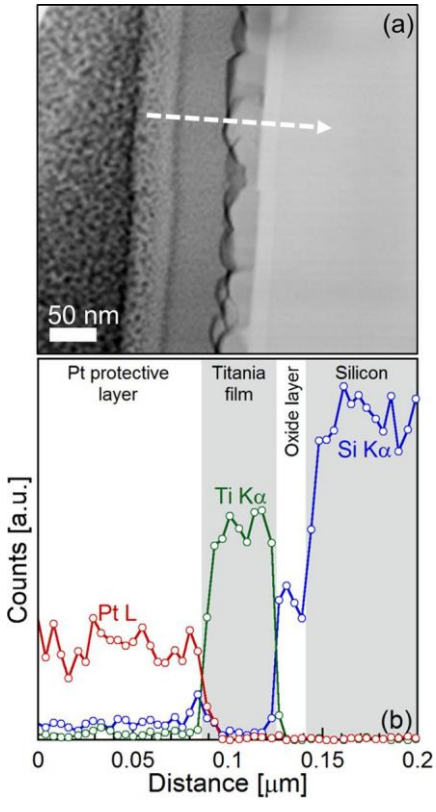

Figure 2. (a) BF-TEM and (b) XEDS line scan of a representative cross section of a thin TiO_2 film prepared by blade-coating of 50 μL of chelated TiO_2 precursor solution at a rate of u = 1.2 cm min^{-1} on the thermally grown oxide layer of a silicon wafer followed by 3 h calcination at 800 °C. The cross section was prepared by focused ion beam (FIB) etching. The Pt L signal derives from the protective surface layer deposited in the FIB etching process.

for TiO_2 films prepared on pristine crystalline Si(100) surfaces,[37,38] our work here clearly shows that a crystalline interface (i.e., registry between the crystalline film and underlying substrate) is not a necessary prerequisite for realizing thin film stabilization.

In addition, while doping of silicon species within TiO_2 is known to inhibit the anatase to rutile transformation,[25] XEDS mapping in Figure 2 did not detect any significant Si Kα signal from within the TiO_2 film or Ti Kα signal within the SiO_2 layer. The low concentrations of Si noted along the top surface of the TiO_2 film are most likely an artifact of the FIB process used to prepare the cross-section sample whereby sputtered material can be redeposited on free surfaces. The clearest indication of this artifact of the FIB process comes from the bulk Pt protective layer, wherein a measurable Si signal is recorded despite this layer being separated from the SiO_2/Si region. While we cannot completely rule out localized elemental doping in the vicinity of the TiO_2/SiO_2 interface, homogeneous elemental doping within the TiO_2 film falls below the detected amount of Si in the Pt region and, thus, below the detectability limit of the XEDS technique (~0.5 wt %). Literature evidence derived from Si-TiO_2 materials prepared by infiltrating a liquid Si source into a TiO_2 sample[43] suggests the need for homo-geneous Si doping at higher levels (ca. 3%) for Si-doping-based resistance to the anatase-to-rutile transformation, suggesting that Si doping is not a primary factor in the thin film stabiliza-tion we observe here.

Lack of Critical Nucleus Size as a Mechanism for Thin Film Stabilization. The thin nature of the TiO_2 film raises the possibility that film stabilization could derive from the physical reduction of crystallite sizes to a level concomitant with the critical radius necessary to effectively balance the surface and bulk free energies of the crystal, a concept established by Garvie for ZrO_2[30−32] that has also been shown to generally apply for TiO_2. This critical radius is typically cited as ca. 15 nm for TiO_2, although the specific critical point varies among literature reports.[44] Scherrer equation analysis of the A(101) and R(110) reflections (Figure 3) helps provide semiquantitative insight

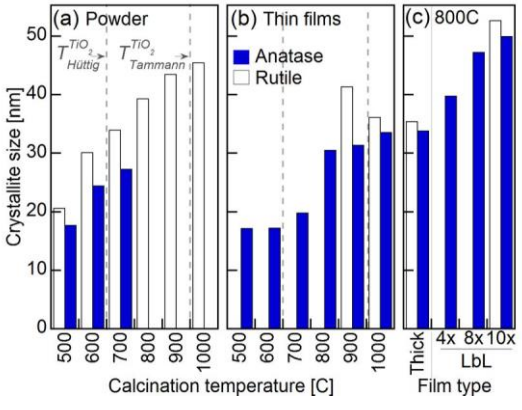

Figure 3. Estimates of anatase (closed bars) and rutile (open bars) polymorph crystal size by XRD Scherrer analysis as a function of calcination temperature for TiO_2 (a) powders and (b) thin films. Whereas "thin" films were prepared at a coating rate of u = 1.2 cm min^{-1}, "thick" films, shown in (c) along with layer-by-layer (LbL) films resulting from 4, 8, and 10 sequential depositions, were prepared at a coating rate of u = 0.12 cm min^{-1}. The absence of a bar denotes the absence of the corresponding polymorph from XRD characterization of the film.

into the comparative size of anatase and rutile crystallites comprising the powders and films within this work. In the case of the bulk powders (Figure 3a), crystallite size increases monotonically with increasing calcination temperature. This is consistent with temperature-induced crystallite coarsening. Rutile crystallites are found to be slightly larger than anatase crystallites, which is consistent with Garvie's thermodynamic theory that larger crystallites prefer the thermodynamically more stable polymorph (i.e., rutile).[30−32] These data suggest that once rutile particles have formed, their growth is faster in powder TiO_2 samples than in the films, since the bulk matrix of agglomerated crystallites in the powders allows unconstrained growth of the rutile polymorph.

In contrast, no apparent growth in size is observed for anatase crystallites in the thin films (Figure 3b) at temperatures below or even at the Hüttig temperature. This underscores the apparent resistance, in the case of the films, to atomic surface mobility as a crystal coarsening mechanism, perhaps owing to the suppression of the number of surface atoms by intimate crystallite attachment to both the underlying substrate and across the grain boundaries between adjacent titania crystallites (Figure 2). This difference ultimately leads to the crystallite size in the films being consistently smaller than that in the powders (Figure 3a) for a given value of calcination temperature.

The maximum mean anatase crystallite size observed for the powders was ca. 27 nm (at 700 °C) before complete conversion to the rutile polymorph occurred. In the case of the thin TiO_2 film, a slightly larger mean crystallite size was reached as a result of a sharp 50% increase in grain size during the 700−800 °C calcination step. However, unlike in the powdered TiO_2 samples,

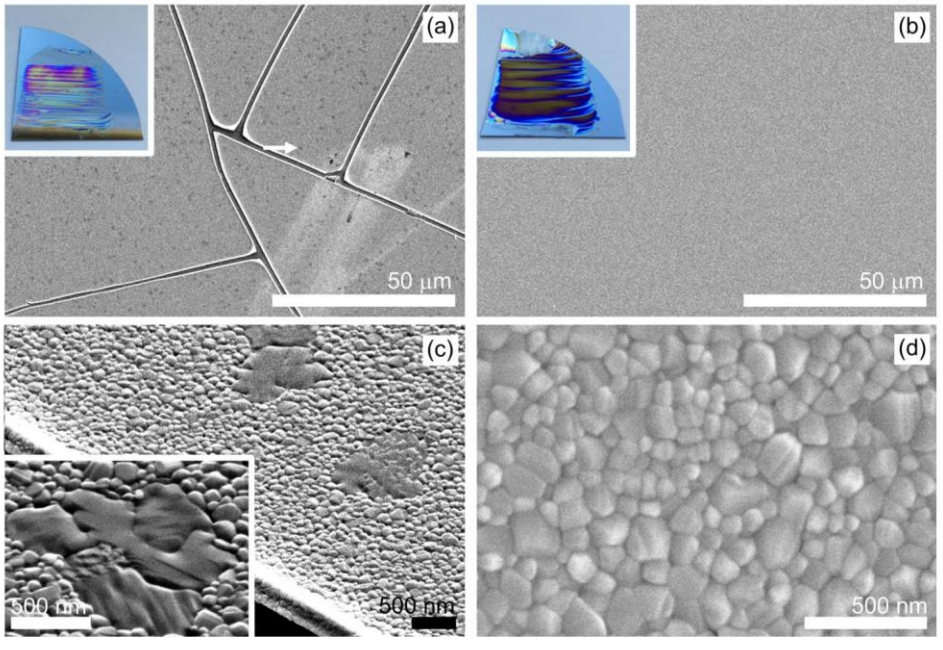

Figure 4. Representative SEM micrographs of (a, c) thick (u = 0.12 cm min^{-1}) and (b, d) thin (u = 1.2 cm min^{-1}) TiO_2 films prepared via convective deposition of 50 μL aliquots of chelated TiO_2 precursor solution on a SiO_2/Si wafer followed by 3 h calcination at 800 °C. Extended platelike domains in (c, inset) are dispersed throughout the thick films as indicated by the arrow in (a) which points to a representative feature.

the film remains purely anatase even after this large increase in mean crystallite size. Only upon reaching the Tammann temperature of titania ($TiO_2^{Tammann}$ ~ 920 °C) are rutile crystallites detected with mean sizes consistent with those in the powder. Ultimately, the large metastable anatase crystallites detected in the thin films suggest that a universal critical nucleus size of around 15 nm cannot be a major factor governing the observed stabilization.

Robustness of TiO_2 Stabilization to Film Thickness: Bridging Thin Films and Bulk Materials. In an effort to bridge thin film character with bulk powders, we have also studied films of increasing thickness, achieved by systematically slowing the rate of convective deposition of the chelated TiO_2 precursor solution. In Figure 1b (dashed diffraction pattern), Figure 1c, and Figure 3c, corresponding data are shown for "thick" TiO_2 films prepared at a coating rate of u = 0.12 cm min^{-1} and calcined at 800 °C. A measurable increase in mean anatase crystallite size even beyond the larger sizes observed for the "thin" films was recorded, and a subtle onset of partial anatase-to-rutile transformation occurs at 800 °C for the thicker sample.

Plan view SEM imaging of the thick (Figures 4a,c) and thin (Figures 4b,d) TiO_2 films reveals differences in film morphology. Namely, the 100% anatase thin films are continuous, intact, and composed of intergrown crystallites; whereas, the thicker films contain cracks deriving most probably from substantial shrinkage of the gel prior to crystallization as capillary effects and syneresis act to contract the alkoxide based gel.[45] Ultimately, Figure S5 shows that delamination of the film along these cracks leads to crystallite coarsening upon high temperature calcination, as the film is no longer constrained by attachment to the surface of the substrate. Additionally, the onset of partial transformation to the rutile polymorph in the thicker films is accompanied by the appearance of elongated, anisotropic crystallites embedded within the polycrystalline films. These platelike crystallites are noticeably absent in the pure anatase thin films when prepared under the same conditions (i.e., 800 °C calcination).

We hypothesize that this increase in film thickness shifts the system more toward bulk powder behavior such that the apparent interfacial stabilization mechanism may be reduced. However, it is remarkable that anatase polymorph stabilization persists to a significant extent even in these thick films, as underscored by the fact that only ~10% interconversion of anatase-to-rutile polymorphs has occurred at 800 °C. This is most likely due to the fact that while some film cracking and associated localized coarsening has occurred, the majority of the film area remains securely adhered to the substrate with intimate boundaries to neighboring grains being maintained.

Beyond Amorphous Substrates: TiO_2 Film Growth atop Crystalline TiO_2 Surfaces. In order to probe if the TiO_2/SiO_2 interface is critical for the observed polymorph stabilization or whether another thin film mechanism may govern the observed phenomenon, we prepared TiO_2 films via layer-by-layer (LbL) convective deposition. Here, the first TiO_2 layer serves to bury the SiO_2 surface so that the second and subsequent layers are effectively deposited onto a non-siliceous (i.e., crystalline TiO_2) substrate. The LbL deposition was achieved by sequential coatings of 20 μL of the chelated TiO_2 precursor solution at a rate of u = 1.2 cm min^{-1} with intermediate calcination to 800 °C after each deposition. SEM characterization (Figure 5c) of the films prepared via this iterative deposition procedure, specifically at a cracked and partially delaminated region within the film, confirms their multilayer morphology.

XRD was used to characterize the LbL films after each layer was deposited and calcined at 800 °C for 3 h (Figure 5a). In the case of the thin films, the anatase polymorph remains stabilized during LbL deposition after successive calcinations at 800 °C as is noted by the presence of the A(101) peak and absence of the R(110) peak. Remarkably, the mean anatase crystallite size in these multilayer films exceeds the mean rutile crystallite size in the powder samples (Figure 3c), again underscoring the apparent lack of a universal critical nucleus size required for hindering the anatase-to-rutile transformation.

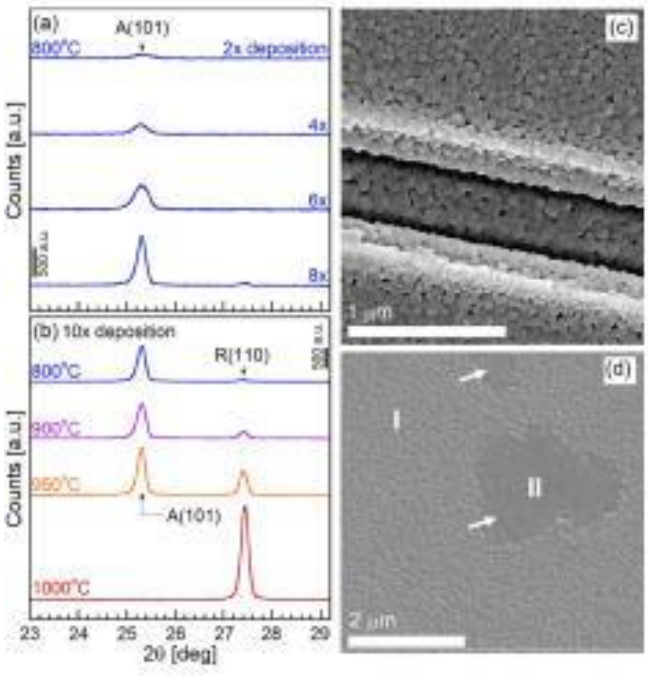

Figure 5. XRD characterization of multilayer TiO_2 films prepared through layer-by-layer blade deposition of 20 μL of chelated TiO_2 precursor sols at a rate of 1.2 cm min^{-1}, with intermediate calcination to 800 °C after each deposition shown in (a) for 2, 4, 6, and 8 depositions. (b) XRD data collected on films prepared via 10 sequential depositions and calcined separately to specified temperatures for 3 h. SEM micrographs show representative views of (c) the top particulate surface and crack revealing the multilayer particulate nature of a film after 5 successive depositions that had been calcined at 800 °C and (d) the top surface of a film prepared by 10 successive depositions that had been finally calcined to 950 °C.

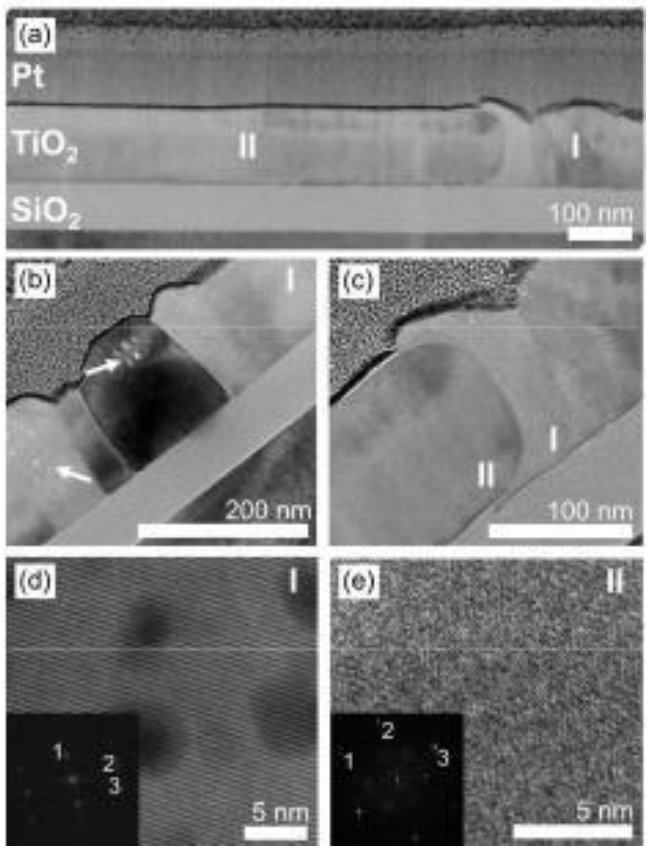

Figure 6. Representative (a) TEM micrograph of FIB cross-sectioned TiO_2 film supported on the thermal oxide layer of a Si wafer prepared by 10 sequential layer-by-layer depositions with intermediate 3 h calcination at 800 °C and final 3 h calcination at 950 °C. The Pt layer is a surface protective layer deposited during the preparation of the FIB cross section. Two representative crystalline regions are present throughout the films, characterized by (a, b, d, region I) columnar crystals along with embedded (a, c, e, region II) extended crystalline domains. Panels d and e show representative lattice images obtained from regions I and II, respectively, along with their corresponding fast Fourier transforms (FFTs) indexed (d) as anatase 1:(101), 2:(020), and 3:(121) (Table S1) and (e) inconclusively as being consistent with both anatase and rutile structures (see Table S2).

The thickest film studied, composed of 10 layers, was cut into four similar sized pieces and calcined at temperatures ranging from 800 to 1000 °C (Figures 5c and 1c). At these temperatures, which approach and exceed the characteristic Tammann temperature of TiO_2, partial transformation to the rutile polymorph emerges. SEM characterization of the top surface of the iteratively deposited films, after high-temperature calcination (800−1000 °C), shows the growth of extended cry-stalline platelets (region II, arrowed in Figure 5d and Figure S6) embedded within the polycrystalline films (region I). When increasing the calcination temperature, XRD analysis shows that the growth of these platelets accompanies gradual development of the rutile polymorph (Figure 5b) indicated by the onset and development of the R(110) reflection. After calcination at 1000 °C, platelet growth (region II) continues until encompass-ing the entire surface of the film (Figure S6), with XRD (Figure 5b) showing the disappearance of the A(101) reflection and, thus, complete transformation to a rutile-pure film.

Further characterization by TEM and STEM of a representative cross section of a thick LbL TiO_2 film prepared via 10 sequential depositions of the precursor solution, iterative calcination at 800 °C, and final calcination at 950 °C is shown in Figure 6. In contrast to the stacked nanoparticulate morphology of the LbL films calcined at 800 °C (Figure 5c), TEM reveals that heating to 950 °C a temperature exceeding the Tammann temperature for TiO_2 leads to textured columnar grains comprising the polycrystalline regions (region I) of the film (Figures 5d and 6a). The difference in the diffraction contrast between adjacent grains is indicative of random in-plane lattice orientations of the crystallites and, thus, no obvious pre-ferential crystal orientation parallel to the substrate plane. TEM (Figure 6a) also shows that the TiO_2 platelets identified as region II in Figure 5d run parallel to the substrate surface.

The formation of columnar crystallites (Figure 6b) appears to derive from sintering and coalescence of the stacked crystallites, likely a result of bulk-to-surface atomic mobilization, and leads to extended crystallization of anatase grains. The structure of the type I columnar grains was confirmed to be anatase by indexing of corresponding lattice images (Figure 6d and Table S1). Void features within the interior of the columnar grains (arrowed in Figure 6b) may be remnants of interstices and porosity from the original particulate LbL films, shown in Figure 5c, that have been partially retained during the film densification associated with the sintering process.

Cross-sectional TEM images reveal that the extended platelike domains (region II) embedded within the polycrystal-line film also span from the surface of the film to the oxide interface. As shown in Figure 6c, these large grains appear to protrude into neighboring crystallites in a fashion indicative of reconstructive transformation. The shape of this intercrystalline

interface indicates the possibility of more rapid grain growth in the interior of the crystal than at either the free surface or the TiO_2/SiO_2 interface, a phenomenon likely accelerated when approaching the characteristic Tammann temperature of TiO_2 where bulk-to-surface atomic mobility would dominate. Index-ing of lattice images (Figure 6e and Table S2) collected from these type II extended domains could not be conclusively assigned to pure anatase or pure rutile polymorphs. However, the platelet formation was found to accompany the onset and evolution of the characteristic rutile reflection by XRD (Figure 5b). The reconstructive nature of the anatase-to-rutile polymorph transformation is consistent with the absence from the extended plate-like domains of void features like those observed in the columnar anatase grains.

XEDS mapping carried out on the thick LbL-derived TiO_2 film after final calcination at 950 °C (Figure S7) shows an overlap of the O Kα signal and both the Ti- and Si-rich regions of the sample, the latter of which appear to be each confined to the TiO_2 and SiO_2 thermal oxide layers, respectively. No homo-geneous silicon doping was detected in the TiO_2 layer at least within the spatial resolution and detectability limits achievable with this technique. Thus, it appears that high-temperature calcination of the thick LbL-derived film at 950 °C did not promote significant silicon doping to the TiO_2, in common with the situation for thinner films calcined at the lower temperature of 800 °C. The slow heating rate (5 °C/min) and 3 h treatment time most likely facilitated thermodynamic relaxation of both the TiO_2 and SiO_2 layers, thus limiting the extent of doping to the immediate vicinity of the TiO_2/SiO_2 interface, as opposed to the phenomenon of kinetic trapping of bulk dopants in semiconductors, for example, which requires ion implantation and rapid thermal processing.[46]

Hypothesized Mechanistic Picture of TiO_2 Film Stabilization. The anatase-to-rutile polymorph transformation of TiO_2 is a reconstructive process requiring bond breaking and atom reconfiguration.[25] This transformation requires the input of sufficient energy to overcome the barrier for conversion of the trapped metastable state (i.e., anatase) into the more thermo-dynamically desirable state (i.e., rutile). This process can occur either by surface driven atomic transport in which metastable anatase crystallites feed growing rutile grains or by internal atomic reconfiguration. In bulk materials, the Hüttig and Tammann temperatures are typically used to define character-istic conditions required for triggering surface and bulk atomic mobility, respectively. In this study, bulk powdered titania samples were observed to undergo the anatase-to-rutile transformation at temperatures consistent with the Hüttig temperature for TiO_2, while thin TiO_2 films were able to resist such a polymorphic transition until reaching the more elevated Tammann temperature.

The key distinctions, revealed in this work, between the polymorph transformations of films versus powders appear to be the confinement of the former to an underlying oxide sub-strate and close proximity of adjacent crystallites. Thus, the film morphology ultimately minimizes exposure of surface atoms, resists atomic surface rearrangement, and effectively limits low temperature driven mechanisms of polymorph transformation. Comprehensive XRD analysis of the films as a function of calcination temperature reveals that the stability of the anatase polymorph is only compromised when the calcination temperature approaches the characteristic Tammann temperature of bulk titania ($TiO_2^{Tammann}$ ~ 920 °C). The concomitant onset of bulk atomic mobility at these elevated temperatures appears to be necessary and sufficient to induce bulk-to-surface transport required for propagative reconstruction of the anatase-to-rutile polymorph. Thus, while localized doping along the TiO_2/SiO_2 interface could assist in stabilization of the interfacial anatase structure, it appears that particle-to-particle and particle−substrate contact serve as key factors contributing to the inherent stabilization of metastable oxide films.

CONCLUSIONS

This work demonstrates a phenomenon which preserves the traditionally metastable anatase crystal structure of titania at elevated temperatures (T > 500 °C) along a TiO_2/SiO_2 interface in thin film structures. While the anatase-to-rutile transformation of bulk TiO_2 powders occurs at temperatures consistent with the characteristic Hüttig temperature of titania ($TiO_2^{Hüttig}$ ~ 610 °C), polymorph transformation within the films is delayed until the Tammann temperature ($TiO_2^{Tammann}$ ~ 920 °C) is reached. The persistence of anatase crystallites, larger than the theoretical size necessary for polymorphic transformation (ca. 15 nm), suggests that particle size does not govern film stabilization. Moreover, stability of the metastable crystallites does not appear to be strongly sensitive to film thickness nor to the specific nature (i.e., crystalline versus amorphous) of the underlying substrate. Instead, whereas surface-driven atomic mobility feeds low-temperature polymorph transformation in bulk, high-surface-area powders, this mechanism seems to be inhibited by the inherent confinement of crystallites in two-dimensional, interface-coordinated arrange-ments within thin films. We show that only when temperatures associated with the onset of bulk-to-surface atomic mobilization are reached is the growth of extended plate-like domains observed and the reconstructive anatase-to-rutile transformation detected.

ASSOCIATED CONTENT

* Supporting Information

Ellipsometry measurements of thermal oxide layer on Si wafers, schematic and SEM micrographs of focused ion beam preparation of $TiO_2/SiO_2/Si$ wafer cross sections, XEDS elemental maps of thin TiO_2 films, SEM micrographs of film delamination and coarsening, SEM micrographs and XEDS maps of LbL films calcined at 800−1000 °C, indexing of lattice fringes (PDF)

AUTHOR INFORMATION

Corresponding Author

*E-mail snyder@lehigh.edu; Ph (610) 758-6834; Fax (610) 758-5057 (M.A.S.).

ORCID

Li Lu: 0000-0002-6688-1176

Mark A. Snyder: 0000-0002-8925-0588

Notes

The authors declare no competing financial interest.

ACKNOWLEDGMENTS

D.G.G. and M.A.S. gratefully acknowledge support for this work as part of the Catalysis Center for Energy Innovation, an Energy Frontier Research Center funded by the U.S. Department of Energy Office of Science, Office of Basic

Energy Sciences, under Award DE-SC0001004. Funding from the National Science Foundation under Grant CBET-1351613 is also gratefully acknowledged for partial support of microscopy studies helping to identify the template-mediated phenomenon. The authors also thank Dr. Robert Keyse (Lehigh University) for guidance when performing FIB milling.

REFERENCES

(1) O'Neill, B. J.; Jackson, D. H. K.; Lee, J.; Canlas, C.; Stair, P. C.; Marshall, C. L.; Elam, J. W.; Kuech, T. F.; Dumesic, J. A.; Huber, G. W. Catalyst Design with Atomic Layer Deposition. ACS Catal. 2015, 5 (3), 1804−1825.

(2) Jiang, C.; Leung, M. Y.; Koh, W. L.; Li, Y. Influences of Deposition and Post-Annealing Temperatures on Properties of TiO_2 Blocking Layer Prepared by Spray Pyrolysis for Solid-State Dye-Sensitized Solar Cells. Thin Solid Films 2011, 519 (22), 7850−7854.

(3) Verbruggen, S. W.; Deng, S.; Kurttepeli, M.; Cott, D. J.; Vereecken, P. M.; Bals, S.; Martens, J. A.; Detavernier, C.; Lenaerts, S. Photocatalytic Acetaldehyde Oxidation in Air Using Spacious TiO_2 Films Prepared by Atomic Layer Deposition on Supported Carbona-ceous Sacrificial Templates. Appl. Catal., B 2014, 160−161 (1), 204− 210.

(4) Vorotilov, K. A.; Orlova, E. V.; Petrovsky, V. I. Sol-Gel TiO_2 Films on Silicon Substrates. Thin Solid Films 1992, 207 (1−2), 180− 184.

(5) Yan, Y.; Chaudhuri, R.; Sarkar, A. Synthesis, Characterizations, and Optical Properties of Stacked Porous Thin Films Derived from Sol-Gel Process. J. Am. Ceram. Soc. 1996, 79 (4), 1061−1065.

(6) Yan, Y.; Chaudhuri, S. R.; Chen, D.-G.; Bolker, B.; Sarkar, A. Microstructural Evolution of Titania Sol-Gel Thin Films. MRS Online Proc. Libr. 1994, 346, 973−978.

(7) Liu, W.; Zhang, B.; Liu, X.; Xu, L. Thermal Stability of Silica-Zirconia Membranes. Chin. J. Chem. Eng. 2006, 14, 31−36.

(8) Phadke, S.; Sorge, J. D.; Hachtmann, S.; Birnie, D. P. Broad Band Optical Characterization of Sol-Gel TiO_2 Thin Film Microstructure Evolution with Temperature. Thin Solid Films 2010, 518 (19), 5467− 5470.

(9) Gao, L.; Wang, Y.; Yan, Y.; Li, Q.; Hao, C.; Ma, T. Enhanced Photoactivities and TiO_2 Particles Induced by Bio-Inspired Micro-Nanoscale Substrate. J. Colloid Interface Sci. 2016, 470, 10−13.

(10) Zainal, Z.; Lee, C. Y. Properties and Photoelectrocatalytic Behaviour of Sol-Gel Derived TiO_2 Thin Films. J. Sol-Gel Sci. Technol. 2006, 37 (1), 19−25.

(11) Shi, L.; Tin, K. C.; Wong, N. B. Thermal Stability of Zirconia Membranes. J. Mater. Sci. 1999, 34 (14), 3367−3374.

(12) Wachs, I. E. Recent Conceptual Advances in the Catalysis Science of Mixed Metal Oxide Catalytic Materials. Catal. Today 2005, 100 (1−2), 79−94.

(13) Takahashi, Y.; Matsuoka, Y. Dip-Coating of TiO_2 Films Using a Sol Derived from $Ti(O\text{-}i\text{-}Pr)_4$-Diethanolamine-$H_2O$-i-PrOH System. J. Mater. Sci. 1988, 23 (6), 2259−2266.

(14) Li, X.; Zhu, P.; Liu, G.; Zhang, J.; Song, R.; Ee, Y.-K.; Kumnorkaew, P.; Gilchrist, J. F.; Tansu, N. Light Extraction Efficiency Enhancement of III-Nitride Light-Emitting Diodes by Using 2-D Close-Packed TiO_2 Microsphere Arrays. J. Dispersion Technol. 2013, 9 (5), 324−332.

(15) Kosacki, I.; Petrovsky, V.; Anderson, H. U.; Colomban, P. Raman Spectroscopy of Nanocrystalline Ceria and Zirconia Thin Films. J. Am. Ceram. Soc. 2002, 85 (11), 2646−2650.

(16) Correa, G. C.; Bao, B.; Strandwitz, N. C. Chemical Stability of Titania and Alumina Thin Films Formed by Atomic Layer Deposition. ACS Appl. Mater. Interfaces 2015, 7, 14816−14821.

(17) Brinker, C. J.; Hurd, A. J.; Schunk, P. R.; Frye, G. C.; Ashley, C. S. Review of Sol-Gel Thin Film Formation. J. Non-Cryst. Solids 1992, 147−148, 424−436.

(18) Brinker, C. J.; Smith, D. M.; Deshpande, R.; Davis, P. M.; Hietala, S.; Frye, G. C.; Ashley, C. S.; Assink, R. A. Sol-Gel Processing of Controlled Pore Oxides. Catal. Today 1992, 14, 155−163.

(19) Davis, P. J.; Brinker, C. J.; Smith, D. M. Pore Structure Evolution in Silica Gel during Aging/Drying I. Temporal and Thermal Aging. J. Non-Cryst. Solids 1992, 142, 189−196.

(20) Davis, P. J.; Brinker, C. J.; Smith, D. M.; Assink, R. A. Pore Structure Evolution in Silica Gel during Aging/Drying II. Effect of Pore Fluids. J. Non-Cryst. Solids 1992, 142, 197−207.

(21) Deshpande, R.; Hua, D.-W.; Smith, D. M.; Brinker, C. J. Pore Structure Evolution in Silica Gel during Aging/Drying. III. Effects of Surface Tension. J. Non-Cryst. Solids 1992, 144, 32−44.

(22) Davis, P. J.; Deshpande, R.; Smith, D. M.; Brinker, C. J.; Assink, R. A. Pore Structure Evolution in Silica Gel during Aging/Drying. IV. Varying Pore Fluid pH. J. Non-Cryst. Solids 1994, 167, 295−306.

(23) Yi, G.; Sayer, M. Sol-Gel Processing of Complex Oxide Films. Am. Ceram. Soc. Bull. 1991, 70 (7), 1173−1177.

(24) Ertl, G.; Knozinger, H.; Weitkamp, J. Spreading and Wetting. In Preparation of Solid Catalysts; Wiley-VCH: Weinheim, 1999; pp 501− 526.

(25) Hanaor, D. A. H.; Sorrell, C. C. Review of the Anatase to Rutile Phase Transformation. J. Mater. Sci. 2011, 46 (4), 855−874.

(26) Wachs, I. E.; Keturakis, C. J. Monolayer Systems. In Comprehensive Inorganic Chemistry II: From Elements to Applications; Elsevier: Amsterdam, 2013; pp 131−151.

(27) Wang, C.-B.; Cai, Y.; Wachs, I. E. Reaction-Induced Spreading of Metal Oxides onto Surfaces of Oxide Supports during Alcohol Oxidation: Phenomenon, Nature, and Mechanisms. Langmuir 1999, 15 (4), 1223−1235.

(28) Takagi, M. Electron-Diffraction Study of Liquid-Solid Transition of Thin Metal Films. J. Phys. Soc. Jpn. 1954, 9 (3), 359−363.

(29) Stevens, R. Zirconia and Zirconia Ceramics; Magnesium Elektron Ltd.: Manchester, UK, 1986.

(30) Garvie, R. C. The Occurrence of Metastable Tetragonal Zirconia as a Crystallite Size Effect. J. Phys. Chem. 1965, 69 (4), 1238−1243.

(31) Garvie, R. C. Stabilization of the Tetragonal Structure in Zirconia Microcrystals. J. Phys. Chem. 1978, 82 (2), 218−224.

(32) Garvie, R. C.; Goss, M. F. Intrinsic Size Dependence of the Phase Transformation Temperature in Zirconia Microcrystals. J. Mater. Sci. 1986, 21 (4), 1253−1257.

(33) Garvie, R. C.; Hannink, R. H.; Pascoe, R. T. Ceramic Steel? Nature (London, U. K.) 1975, 258, 703−704.

(34) Kingery, W. D. Boundary Stresses. In Introduction to Ceramics; Wiley: New York, 1960; pp 201−203.

(35) Harmer, M. P. The Phase Behavior of Interfaces. Science (Washington, DC, U. S.) 2011, 332, 182−183.

(36) Gorbenko, O. Y.; Samoilenkov, S. V.; Graboy, I. E.; Kaul, A. R. Epitaxial Stabilization of Oxides in Thin Films. Chem. Mater. 2002, 14, 4026−4043.

(37) Selvaraj, U.; Prasadarao, A. V.; Komarneni, S.; Roy, R. Sol-Gel Fabrication of Epitaxial and Oriented TiO_2 Thin Films. J. Am. Ceram. Soc. 1992, 75 (5), 1167−1170.

(38) Legrand-Buscema, C.; Malibert, C.; Bach, S. Elaboration and Characterization of Thin Films of TiO_2 Prepared by Sol-Gel Process. Thin Solid Films 2002, 418 (2), 79−84.

(39) Bradley, D. C.; Mehrotra, R. C. Metal Alkoxides; Academic Press: London, UK, 1978.

(40) Kumnorkaew, P.; Ee, Y. K.; Tansu, N.; Gilchrist, J. F. Investigation of the Deposition of Microsphere Monolayers for Fabrication of Microlens Arrays. Langmuir 2008, 24 (21), 12150− 12157.

(41) Spurr, R. A.; Myers, H. Quantitative Analysis of Anatase-Rutile Mixtures with an X-Ray Diffractometer. Anal. Chem. 1957, 29 (5), 760−762.

(42) Cullity, B. D. Diffraction I: The Direction of Diffracted Beams. In Elements of X-ray Diffraction; Addison-Wesley Publishing Company: Reading, MA, 1956; pp 96−102.

(43) Okada, K.; Yamamoto, N.; Kameshima, Y.; Yasumori, A.; MacKenzie, K. J. D. Effect of Silica Additive on the Anatase-to-Rutile Phase Transition. J. Am. Ceram. Soc. 2001, 84 (7), 1591−1596.

(44) Ranade, M. R.; Navrotsky, A.; Zhang, H. Z.; Banfield, J. F.; Elder, S. H.; Zaban, A.; Borse, P. H.; Kulkarni, S. K.; Doran, G. S.;

Whitfield, H. J. Energetics of Nanocrystalline TiO_2. Proc. Natl. Acad. Sci. U. S. A. 2002, 99, 6476−6481.

(45) Boettcher, J. M.; Joy, M.; Joshi, K.; Muangnapoh, T.; Gilchrist, J. F. Spacing of Seeded and Spontaneous Streaks during Convective Deposition. Langmuir 2015, 31 (40), 10935−10938.

(46) Hamm, R. W.; Hamm, M. E. Ion Implantation for Fabrication of Semiconductor Devices and Materials. In Industrial Accelerators and Their Applications; World Scientific: Hackensack, NJ, 2012; pp 9−54.